communications physics

ARTICLE

https://doi.org/10.1038/s42005-023-01414-7 OPEN

X-ray induced Coulomb explosion imaging of transient excited-state structural rearrangements in CS_2

James Unwin[1,18], Felix Allum[1,2,3,18✉], Mathew Britton[2,3], Ian Gabalski[3,4], Hubertus Bromberger[5], Mark Brouard[1], Philip H. Bucksbaum[3,4,6], Taran Driver[2,3], Nagitha Ekanayake[5], Diksha Garg[5], Eva Gougoula[5], David Heathcote[1], Andrew J. Howard[3,4], Paul Hockett[7], David M. P. Holland[8], Sonu Kumar[5,9], Chow-shing Lam[1], Jason W. L. Lee[5], Joseph McManus[1], Jochen Mikosch[10], Dennis Milesevic[1], Russell S. Minns[11], Christina C. Papadopoulou[5], Christopher Passow[5], Weronika O. Razmus[11], Anja Röder[12], Arnaud Rouzée[12], Michael Schuurman[7,13], Alcides Simao[14], Albert Stolow[7,13,15,16], Atia Tul-Noor[5], Claire Vallance[1], Tiffany Walmsley[1], Daniel Rolles[17], Benjamin Erk[5], Michael Burt[1✉] & Ruaridh Forbes[2✉]

Structural imaging of transient excited-state species is a key goal of molecular physics, promising to unveil rich information about the dynamics underpinning photochemical transformations. However, separating the electronic and nuclear contributions to the spectroscopic observables is challenging, and typically requires the application of high-level theory. Here, we employ site-selective ionisation via ultrashort soft X-ray pulses and time-resolved Coulomb explosion imaging to interrogate structural dynamics of the ultraviolet photochemistry of carbon disulfide. This prototypical system exhibits the complex motifs of polyatomic photochemistry, including strong non-adiabatic couplings, vibrational mode couplings, and intersystem crossing. Immediately following photoexcitation, we observe Coulomb explosion signatures of highly bent and stretched excited-state geometries involved in the photodissociation. Aided by a model to interpret such changes, we build a comprehensive picture of the photoinduced nuclear dynamics that follows initial bending and stretching motions, as the reaction proceeds towards photodissociation.

[1] Chemistry Research Laboratory, Department of Chemistry, University of Oxford, Oxford OX1 3TA, UK. [2] Linac Coherent Light Source, SLAC National Accelerator Laboratory, Menlo Park, CA 94025, USA. [3] Stanford PULSE Institute, SLAC National Accelerator Laboratory, Menlo Park, CA 94025, USA. [4] Department of Applied Physics, Stanford University, Stanford, CA 94305-4090, USA. [5] Deutsches Elektronen-Synchrotron DESY, Notkestr. 85, 22607 Hamburg, Germany. [6] Department of Physics, Stanford University, Stanford, CA 94305-4013, USA. [7] National Research Council Canada, Ottawa, ON K1A 0R6, Canada. [8] Daresbury Laboratory, Daresbury, Warrington, Cheshire WA4 4AD, UK. [9] Department of Physics, Universität Hamburg, Jungiusstraße 9, 20355 Hamburg, Germany. [10] Institut für Physik, Universität Kassel, Heinrich-Plett-Straße 40, 34132 Kassel, Germany. [11] School of Chemistry, University of Southampton, Highfield, Southampton SO17 1BJ, UK. [12] Max-Born-Institute, Max-Born-Straße 2A, 12489 Berlin, Germany. [13] Department of Chemistry and Biomolecular Sciences, University of Ottawa, 150 Louis Pasteur, Ottawa, ON K1N 6N5, Canada. [14] Ruhr-Universität Bochum, Fakultät für Chemie und Biochemie, Organische Chemie II, Universitätsstraße 150, 44801 Bochum, Germany. [15] Department of Physics, University of Ottawa, 150 Louis Pasteur, Ottawa, ON K1N 6N5, Canada. [16] NRC-uOttawa Joint Centre for Extreme Photonics, Ottawa, ON K1A 0R6, Canada. [17] J. R. Macdonald Laboratory, Department of Physics, Kansas State University, Manhattan, KS 66506, USA. [18] These authors contributed equally: James Unwin and Felix Allum. ✉email: fallum@stanford.edu; michael.burt@chem.ox.ac.uk; ruforbes@stanford.edu

Understanding transient structural rearrangements during photochemical processes is a key step in building a mechanistic picture of chemical and biological processes, such as vision and photosynthesis[1,2]. Ultrafast lasers, spanning the infrared to the X-ray regime, are critical enabling tools to image the excited-state motion of molecular systems on their natural femtosecond timescales[3,4]. In recent years the use of diffractive imaging techniques such as ultrafast electron and X-ray diffraction have provided new insights into excited-state structural changes[4,5]. Alongside these diffractive imaging techniques, Coulomb Explosion Imaging (CEI) with femtosecond laser pulses has emerged as a complementary method to image structural dynamics[6–10]. In notable contrast to diffractive imaging techniques, CEI can exhibit a high sensitivity to light atoms (which have low scattering cross sections), and access high-order structural correlations (i.e., beyond pair distribution functions)[11]. These emerging structural dynamics techniques promise to enable the measurement of ultrafast nuclear dynamics in isolated molecules with high specificity. As such, they offer complementary information to methods such as time-resolved photoelectron spectroscopy and time-resolved X-ray absorption spectroscopy, which are sensitive to both nuclear and electronic dynamics[3,12]. However, fully disentangling the influence of electronic and nuclear dynamics on these spectroscopic observables is often challenging, and interpretation requires the application of high-level theory[13]. It is hoped that by combining the insights from these different techniques, a more complete picture of the coupled nuclear and electronic dynamics at the heart of molecular photochemistry can be determined.

Coulomb explosion is initiated by the rapid removal of multiple electrons from a parent molecule. The resulting strong internal Coulombic repulsion then causes the multiply charged molecule to explode into ionic fragments. The recorded fragment momenta are correlated to the nuclear geometry of the molecules at the time of multiple ionisation. In many cases, the relative fragment momenta arising from a Coulomb explosion can be understood in terms of simple classical simulations of repelling point charges, whilst in other cases, particularly for lower total charge states, more complex ab initio theory may be required[14–16]. Time-resolved Coulomb explosion imaging has found applications in investigating vibrational wavepacket motion[6,17], dissociation[7,8,18] and isomerisation dynamics[19], as well as roaming[10]. Typically, in laboratory-based CEI experiments, intense near-infrared (NIR) pulses are used to initiate Coulomb explosion. Significant strengths of this approach include the ability to approach very high time resolution through use of few-cycle pulses, capitalising on the non-linear nature of the ionisation process itself[20]. However, particularly for longer-duration NIR pulses, nuclear motion within the laser field prior to Coulomb explosion can complicate the interpretation of these experiments. Such motion can be very substantial and may arise due to the sequential nature of strong-field ionisation[7,21] (prompting dynamics involving intermediate charge states), light-induced coupling of different potentials[22], and the strong and very non-linear coordinate-dependence of the strong-field ionisation rate (leading to 'enhanced ionisation' phenomena)[23]. Consequently, the mapping of initial nuclear structure to final fragment momenta is often complex, and potentially intractable. Multiple ionisation with soft X-ray laser pulses, as produced by Free-Electron Lasers (FELs), may minimise such issues. Photoionisation from a core orbital, followed by Auger-Meitner decay(s), rapidly populates the high charge states required to prompt Coulomb explosion. The negligible ponderomotive potentials of intense X-ray pulses places the light-matter interaction in the multiphoton rather than the strong-field ionisation regime. Furthermore, the ionisation cross section typically does not (in the absence of resonances) exhibit a highly non-linear nuclear coordinate dependence. As such, short-wavelength FELs are rapidly emerging as very promising light sources for CEI[11,24].

The target system of the present study, CS_2, is chosen due to its well-studied and complex non-adiabatic ultraviolet (UV) photodynamics, which are discussed shortly. While the NIR-induced dynamics of CS_2 have been studied extensively[25–27], as have those of isovalent CO_2[28–30], the present work represents the first application of time-resolved CEI to the UV-induced dynamics of CS_2. These previous CEI experiments have also demonstrated the significant challenges with traditional intense NIR-based probing. Namely, field-induced couplings of electronic states prompts motion along the bending coordinate, and Coulomb explosion occurs at substantially extended bond-lengths due to enhanced ionisation. By initiating Coulomb explosion through soft X-ray multiphoton ionisation, these deleterious processes are avoided, giving the present work exquisite sensitivity to nuclear structure prior to Coulomb explosion.

Photoexcited CS_2 exhibits many processes of fundamental importance in ultrafast photochemistry, leading ultimately to sub-picosecond photodissociation into both singlet and triplet sulfur atoms, and their correlated CS fragments. Multiple studies have found that production of the spin-forbidden triplet state is dominant, with a branching ratio of approximately 2:1 compared to the spin-allowed singlet sulfur atom[31]. This triplet-dominated branching ratio has recently been ascribed to the rapid formation of a metastable intermediate via internal conversion, which then undergoes intersystem crossing to subsequently produce the triplet sulfur product[32,33]. Prior to dissociation, excited CS_2 undergoes large amplitude bending and stretching[34–37]. Several values for the mean bend angle that the excited molecule adopts have been reported, ranging from 115°[38] to 153°[39]. Quantum beats have also been observed in the ultrafast studies[32,35,40,41] and attributed to quasi-bound dynamics along the stretch and bend coordinates, prompted by the coherent population of multiple vibronic transitions with sufficiently broadband pump pulses. Differences in observations within the wealth of previous studies are potentially attributable to the probe pulses used (defined by pulse wavelength, bandwidth and duration), which result in different observation windows in nuclear configuration space, although use of different pump pulses—hence initial wavepacket properties—also play a role. Conversely, spectroscopic (nanosecond) photoproduct studies were able to resonantly probe the distribution of final product states, but did not observe the ultrafast dissociation dynamics directly[42–44]. Significant recent progress has been made through ultrafast photoelectron spectroscopy measurements employing ultrafast vacuum ultraviolet (VUV) probes to allow valence ionisation along the entire reaction coordinate[32,33]. Here, we extend such ideas further, utilising a soft X-ray probe to study the ultrafast nuclear dynamics through core ionisation, further decoupling the probe process from the (evolving) electronic structure of the photoexcited neutral or final ionised state, giving the present CEI scheme highly specific sensitivity to nuclear dynamics.

Theoretically, the neutral excited-state dynamics have proven particularly difficult to describe accurately since in addition to multiple non-adiabatically coupled singlet states, there is strong coupling to the triplet manifold as well; and all channels involve dissociation. Furthermore, there is a pronounced difference of the wavepacket dynamics on the pump wavelength, as transitions to different vibronic levels of the initially populated $^1\Sigma_u^+$ state are accessed[31]. The combination of all these factors make for exceedingly difficult first-principles simulations, and previous work has necessitated the use of very high, benchmark-quality ab initio computation to achieve even qualitatively correct results[13,37,45]. Even in these studies, treating the nonadiabatic and spin-orbit coupling (e.g. intra-singlet dynamics and intersystem crossing

dynamics) on equal footing was either not attempted[13,45], or treated using more approximate semi-classical methods[37,46,47]. In light of this, one major aim of the present work is to interpret the relationship between the observed time-resolved signals and the nuclear dynamics of photoexcited CS_2 without the input of ab initio theory.

In the current work, a 201.5 nm UV pump pulse excites the CS_2 sample prior to multiple ionisation by a 6.9 nm soft X-ray pulse, which initiates Coulomb explosion predominantly through ionisation from the S 2p orbital followed by Auger-Meitner decay(s)[48,49]. The use of CEI in this experiment allows the excited-state nuclear dynamics of CS_2 to be followed as it proceeds along its reaction coordinate from the predominantly linear ground state geometry, to its bent and stretched excited state, before rapidly decaying to dissociated products. This evolution of the nuclear geometry along non-adiabatically coupled excited electronic states of importance is shown schematically in Fig. 1. Underlying surfaces simulated at the level of theory as described by Wang et al.[45], are shown to illustrate the driving forces of these photoinduced nuclear dynamics. More detail on the previous calculation of these surfaces is given in the Supplementary Methods. For simplicity, and to give purely a general overview of the excitation and dissociation process, only relevant singlet states are shown, although we emphasise that triplet states contribute to the final dissociation process[31]. We further emphasise that calculated potential energy surfaces are not used in interpreting the experimental results of the current work, but provide a useful picture of the forces acting on the molecule and the types of structure that can be expected to be sampled as the molecules dissociate. The structural insights extracted from the experiment are enhanced by the use of three-dimensional covariance analysis to extract relative momenta of pairs of ions produced in a given Coulomb explosion process[50,51]. To further disentangle the large number of soft X-ray-induced fragmentation channels sampled in the experiment, and to relate their appearance to the underlying UV-induced photochemistry, we employ simple Coulomb explosion simulations. These simulations employ a kinetic model of the photodissociation, involving sampling of geometry distributions associated with the ground state and initially populated photoexcited species, which decay to photodissociation products. This approach offers significant insights into the ultrafast nuclear dynamics without the need for challenging, and often infeasible high-level theoretical calculations. Collectively, the current results demonstrate the power of X-ray induced CEI to directly probe the transient structure and ultrafast dynamics of photoexcited species.

Results

Signatures of the UV-induced dynamics of interest are observed in the delay-dependent 3D momentum distributions for a range of ions produced in the experiment. The following discussion focuses on the S^+ and S^{2+} ions, which are sufficient to extract a detailed picture of the photoinduced dynamics in CS_2. A more complete set of delay-dependent momentum distributions of $S^{(3-4)+}$, $C^{(1-2)+}$ and $CS^{(1-2)+}$, as well as static and time-resolved mass spectra, are presented in Supplementary Notes 1, 2 and 3.

S^+ momentum distributions. Firstly we turn to the delay-dependent momentum distribution of S^+. As the experiment employs soft X-ray ionisation above the S 2p edge, which is followed by up to two Auger-Meitner decays, S^+ is unlikely to be produced from X-ray ionisation of isolated sulfur atoms[49]. Consequently, S^+ is predominantly produced following multiple ionisation and fragmentation of either bound CS_2 molecules or CS photoproducts, as charge can be effectively redistributed across the molecule, regardless of the initial core ionisation site[52].

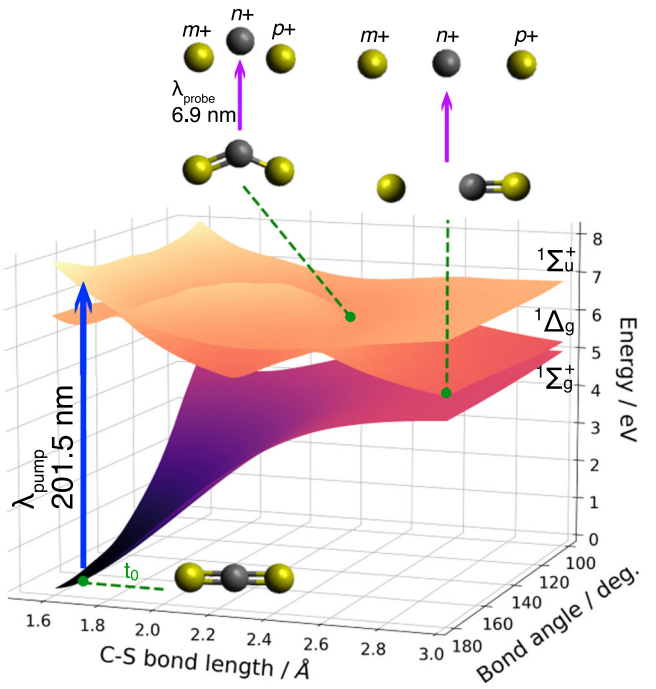

Fig. 1 Schematic representation of the reaction pathway followed by a photoexcited CS_2 molecule. Simulated singlet potential energy surfaces for CS_2, showing the $^1\Sigma_g^+$, $^1\Delta_g$ and $^1\Sigma_u^+$ states[45]. The molecule is excited from the ground state to the optically bright $^1\Sigma_u^+$ state by the 201.5 nm pump pulse. For the sake of simplicity, photoexcitation is shown to occur from a linear ground state geometry. Example molecular geometries and fragments produced following Coulomb explosion are shown at particular locations along the excited-state potential energy surfaces. Grey denotes carbon, yellow sulfur.

Signal arising from Coulomb explosion of excited-state CS_2 molecules prior to dissociation therefore appears more clearly in the S^+ ion in contrast to the S^{2+} ion, where there is a much greater contribution from ionisation of dissociated S atoms, as is discussed shortly.

Figure 2a presents the experimental delay-dependent S^+ ion momentum distribution. Here, and throughout the manuscript, the differential signal is plotted and obtained by subtracting momenta for pump-probe delays where the FEL precedes the UV by 200–700 fs. The unsubtracted momentum distributions for all ions are provided in Supplementary Note 2. Various depletions occur following photoexcitation due to a reduction in the number of ground-state CS_2 molecules that interact with the soft X-ray probe. In addition to these depletions, several enhancements stand out in Fig. 2. These include i) enhancement between ~110 and 180 a.u. for the first several hundred femtoseconds following photoexcitation, and ii) an enhancement at 90 a.u. and below, which persists to long pump-probe delays. These signals can be related to Coulomb explosions of excited CS_2 prior to photodissociation, and of CS fragments produced in the photodissociation, as we will show in the following.

Experimentally, numerous fragmentation channels are observed, originating from a range of parent charge states produced following interaction with the soft X-ray probe pulse. To aid in the assignment of these features and to unravel their relative contributions, we compare the experimental data with simulations of the photodissociation process and subsequent probing by soft X-ray Coulomb explosion. Despite the simplicity of the modelling, strong qualitative agreement between the experimental and simulated (Fig. 2b) delay-dependent momentum distributions is observed by appropriate selection of several parameters, namely:

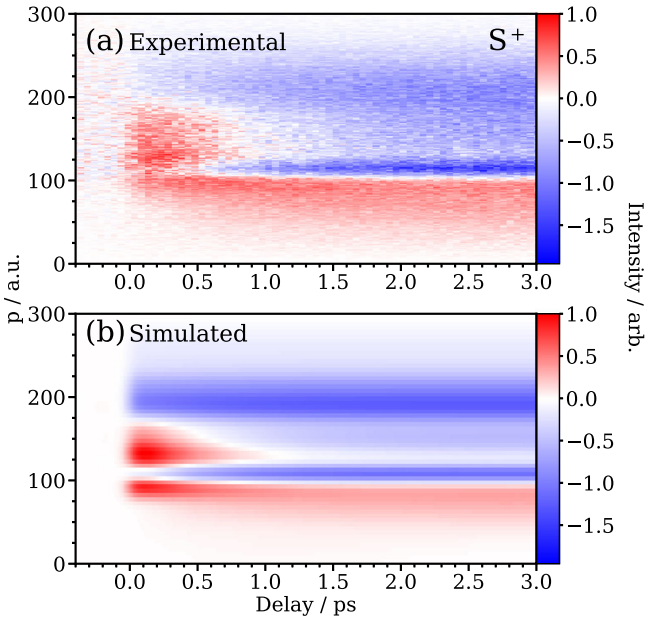

Fig. 2 Delay-dependent difference momentum distribution of the S^+ ion. **a** Experimental and **b** simulated delay-dependent difference momentum distribution of the S^+ ion. Red signal corresponds to enhancements, blue to depletions, relative to pump-probe delays in which the X-ray probe preceeds the UV pump. The simulation is produced from summing the nine fragmentation channels that produce an S^+ ion. A channel-resolved figure showing the individual channels that produce the simulated data is shown in Supplementary Note 7. Momentum is given in atomic units (a.u.).

the geometries of the ground-state and excited-state species, the photodissociation timescale and the relative weightings of different photoionisation and fragmentation channels following soft X-ray ionisation.

The modelling process, which relies on a simple physical picture of the predissociation dynamics of CS_2, but does not rely on high-level theoretical input, is described in detail in the Methods section, but is outlined here briefly. The photodissociation process was modelled assuming exponential kinetics with a single lifetime, yielding S and CS photoproducts which recoil with a Kinetic Energy Release (KER) sampled from a Gaussian distribution similar to that observed experimentally, and Coulombic repulsion is simulated at a series of pump-probe delays by placing point charges at the atomic positions and allowing these to repel classically. The simulation includes a geometry change from an approximately linear to bent structure for excited molecules. Whilst a more-complete kinetic model of the UV photodynamics requires multiple time constants, representing dissociation lifetimes of the singlet and triplet dissociation channels[32,33], here we adopt a simpler scheme given the limited ability for the present experiment to determine a precise delay-dependent singlet and triplet branching ratio (due to their heavily overlapping velocity distributions[42,43]). The limitations of the singlet-triplet ratio determination are explored in greater detail in Supplementary Note 6.

Differing charge state distributions for ionisation of bound CS_2 and dissociated CS and S were included for each of the ten ionisation channels used in these simulations, to account for differing charge localisation following S 2p ionisation in the bound or dissociated species. Table 1 lists the observed channels and indicates their relative weightings, which were chosen to optimise the agreement between simulation and experiment. The channels listed in Table 1 can be interpreted as follows: after dissociation occurs, the two sulfur atoms are no longer equivalent,

Table 1 Coulomb explosion simulation fragmentation channels.

No.	Bound (*q*,*w*)/(*m*,*n*,*p*)	Dissociated (*m*,*n*,*p*)	Probability (%)
1	(1,1)	(2,0,0)	12.5
2	(1,1,1)	(0,1,2)	17.5
3	(2,1,1)	(2,1,1)	15.0
4	(2,1,2)	(2,1,2)	7.5
5	(2,0,1)	(3,0,0)	10.0
6	(1,0,1)	(2,0,0)	5.0
7	(1,1,0)	(0,0,2)	5.0
8	(1,1)	(0,1,1)	15.0
9	(1,0,1)	(0,1,1)	7.5
10	(1,1,1)	(3,0,0)	5.0

Fragmentation channels specified for the Coulomb explosion simulations. These are specified by charges (*m*,*n*,*p*) for three-body Coulomb explosions of either S_a-C-S_b (bound) or S_a+CS_b (dissociated) into S_a^{m+}+C^{n+}+S_b^{p+} and charges (*q*,*w*) for two-body Coulomb explosion into S^{q+}+CS^{w+}. Channel probabilities were determined by empirical fitting.

as one is dissociated (S_a), whilst the other is bound in the CS fragment (S_b). Two sets of charge states are given for each channel, corresponding to the charge state distribution at the limiting short and long C-S_a bond distances, respectively. In the limit of short C-S_a, the molecule is assumed to be 'bound', and charge can redistribute following S 2p ionisation, whilst for extended C-S_a, charge will remain localised at the fragment containing the ionised sulfur. In Table 1 and the remainder of the manuscript, three-body fragmentations are described as (*m*,*n*,*p*), which corresponds to the charge of S_a, C and S_b ions, respectively. Two-body fragmentations are described as (*q*,*w*), which corresponds to the charge on S and CS, respectively. To account for structural dynamics prior to dissociation, differing geometry distributions were assumed when simulating the Coulomb explosion of ground-state CS_2 and excited, but undissociated CS_2.

Analysing the simulated S^+ signal and comparing it to the experimental data in Fig. 2a confirms that the 'transient' enhancements in the 110–180 a.u. region arise primarily from a reduction of the momentum imparted to the S^+ ion in (1,0,1), (1,1,1), and (2,1,1)/(1,1,2) Coulomb explosions following photoexcitation. This is ascribed to two factors. Firstly, stretching of the C-S bonds in the excited state lowers the total KER of these Coulomb explosion channels. Secondly, excited-state bending of CS_2 results in the partitioning of more momentum from the Coulomb explosion into the C^+ ion (as seen in the time-resolved C^+ momentum distribution shown in Supplementary Note 3), and consequently less into the S^+ ion. This can be intuitively understood by considering the limiting case of a purely Coulombic (1,1,1) explosion of a perfectly linear CS_2, in which the C^+ would have zero momentum.

Multiple previous studies have reported lifetimes of the excited state, with Farmanara et al. reporting a lifetime of 380 ± 20 fs at an excitation wavelength of 200.7 nm, as probed by multiphoton ionisation in the NIR[39]. By contrast, under UV (201.3 nm) pump - UV (~267 nm) probe conditions, a biexponential decay was observed, which included a fast component with ~40 fs lifetime (which was assigned to contributions from hot band transitions from initially vibrationally excited ground-state CS_2), and a slower component with a lifetime which varied between 510 fs and 640 fs for different relative polarisations of the two pulses[40]. In the recent time-resolved VUV photoelectron spectroscopy study of Suzuki and coworkers, where a broader bandwidth UV pump pulse centred at ~200 nm was used, a $^1B_2$ lifetime of 630 fs was reported[32], similar to the 570 fs determined by Minns and coworkers in a similar experimental scheme employing relatively

narrow-band pulses[33]. While such lifetimes are in reasonable agreement with the value of 500 fs found here by matching the output of our model to the experimental data, we must stress that the physical meaning of such a lifetime depends on the probe process, the experimental observable and the modelling used to interpret the experimental observations[32,33]. Similarly, given the existence of multiple vibronic transitions with different lifetimes (e.g., as determined from linewidth measurements, which yield a 500 ± 100 fs lifetime for the transition at 201.2 nm[31]), the spectral content of the pump pulse may significantly affect the observed timescales.

At S^+ momenta of ~100 a.u. and below, enhancements are observed following photoexcitation. The primary contribution to this is Coulomb explosion of dissociated CS fragments into $S^+ + C^+$. The higher momentum signal associated with this process overlaps strongly with depletions of Coulomb explosion channels of bound CS_2, most notably the (1,1) Coulomb explosion (simulated channels 1 and 8), which results in a depletion at ~110 a.u. Once more, this signature of Coulomb explosion of the CS fragment is well reproduced by the simulations, if a sufficiently broad distribution of C-S bond lengths is assumed (1.8 Å mean with 0.4 Å standard deviation), consistent with probing a vibrationally hot CS fragment, as observed previously in nanosecond velocity-map imaging measurements[42,44].

S^+ covariance analysis. The assumed bending motion in the excited state can be confirmed by examining the time-dependent angular correlations between the S^+ and C^+ ions. These correlations can be extracted from the data using covariance analysis, as detailed in the Methods section and in previous publications[51,53]. Due to superior signal-to-noise, we present two-fold covariance analysis, representing the correlations between a pair of ions. Figure S23 in Supplementary Note 11 shows example three-fold covariance analysis, in which delay-dependent signal arising from Coulomb explosion of bent excited-state species can also be resolved. Figure 3 shows experimental and simulated covariances for two different ions pairs, (S^+,S^+) and (S^+,C^+), plotted as a function of their relative angle and the sums of the magnitudes of their momenta. As in Fig. 2, data is plotted as a difference signal, following subtractions of the UV late data. Due to limited statistics, we are unable to extract statistically-robust relative momentum distributions finely resolved over pump-probe delay. Consequently, the two-dimensional covariance histograms for each set of ions are shown integrated over two coarse delay regions defined with respect to the temporal overlap of the two pulses: immediately after overlap (<0.7 ps), and longer delays (>1.7 ps). At these delay ranges, the pump-probe signal is dominated by ionisation of photoexcited CS_2 and its dissociated fragments, respectively.

The experimental and simulated covariance images for the (S^+,S^+) ion pair are shown in Fig. 3a, b for delay <0.7 ps and primarily exhibit contributions from two channels:, namely the (1,1,1) and (1,0,1) Coulomb explosion of bound CS_2. Immediately following photoexcitation, the (S^+,S^+) covariance shows transient enhancements at relatively small recoil angles (~130° for the (1,1,1) channel) (Fig. 3b). This provides unambiguous evidence for the (transiently) bent structure of photoexcited CS_2. As expected, the summed S^+ momentum of ~230–360 a.u. is double that of the transient enhancement observed in the time-resolved S^+ momentum distributions discussed previously. As shown in Figure S7 of the SI, this signal is not observed at long pump-probe delays, as expected for this transient excited-state feature. We note that the precise summed momentum and relative angle associated with this feature are sensitive to the bond lengths and angles in the excited state. Figure 3e, f show 1-dimensional projections of the difference covariance signal as a function of recoil angle, and summed momentum respectively. These demonstrate the broad agreement between experiment and simulation, observed for a simulated ensemble of excited-state structures with mean C-S length and S-C-S angles of 2.2 Å and 135°, respectively. Similarly, Fig. 3i presents the integrated covariance signal as a function of pump-probe delay for regions in the two-dimensional covariance histograms corresponding to the transient feature, and from ground state Coulomb explosion. As reproduced by the modelling, a prompt depletion in the ground state signal is observed, as well as a rapid rise and subsequent decay of the transient. In general, the experimental data are more broadly distributed in momentum and recoil angle than the simulation. This is due in part to the finite momentum resolution of the spectrometer, but also due to the simplicity of how the Coulomb explosion is simulated in the model, which neglects deviations from Coulombic forces and assumes instantaneous charging of the molecule. The mean bend angle of 135° reported here is also consistent with the reported degree of early bending in the ab initio multiple spawning computational study performed by Wang et al.[54]. However, we must caution that the phenomenological geometry distributions used in the modelling to reproduce the experimental signal physically represent a combination of the geometries prior to Coulomb explosion, and the deviations of the 'true' Coulomb explosion process from that of our simulation. More detailed theoretical work, particularly in a full simulation of the X-ray induced Coulomb explosion process, will be required to separately discuss these factors.

The covariance analysis for the (S^+, C^+) ion pair identifies signal arising from Coulomb explosion of the dissociated CS photoproduct into C^+ and S^+ at longer pump-probe delays. In Fig. 3c, an enhancement is observed at ~225 a.u. total momentum and 140–180°. Figure S7 in Supplementary Note 4 shows the (S^+, C^+) covariance for shorter delay values (0-0.7 ps), and again shows the absence of the discussed signal, as most of the events at short delays result from the Coulomb explosion of bound molecules. This can be seen in the delay-resolved covariances shown in Fig. 3j, where a gradual increase in the signal assigned to CS Coulomb explosion from zero intensity is seen starting from ~0.2 ps, consistent with the kinetic modelling. The broad range of momenta associated with this signal implies a wide distribution of bond lengths of the probed CS fragment, consistent with considerable vibrational excitation resulting from the photodissociation[42,44]. In this case, the covariance analysis cleanly isolates the enhancements from Coulomb explosion of CS from the various depletions of soft X-ray Coulomb explosion channels produced from CS_2 (see Supplementary Note 9), representing an advantage over examining the uncorrelated S^+ momentum distribution. This is enabled by the vastly different recoil angles associated with these processes. In the direct X-ray Coulomb explosion of the undissociated molecule, C^+ and S^+ are emitted at roughly 100° from one another, while the Coulomb explosion of CS products yields recoil angles closer to 180°. Typically, for two-body Coulomb explosion, a recoil angle distributed narrowly around 180° is to be expected. However, in this case, the CS fragment acquires significant momentum from the initial photodissociation, broadening the distribution of relative angles following Coulomb explosion, as the initial photodissociation and Coulomb explosion may impart momenta along different directions. Such observations are well reproduced by the simulated data shown in Fig. 3d, once more lending confidence to our assignments. This comparison can be examined in more detail by considering one-dimensional projections of the covariance signal, shown in Fig. 3g, h. The agreement observed supports our choice of values used for generating the simulations, and hence our subsequent feature assignments using those

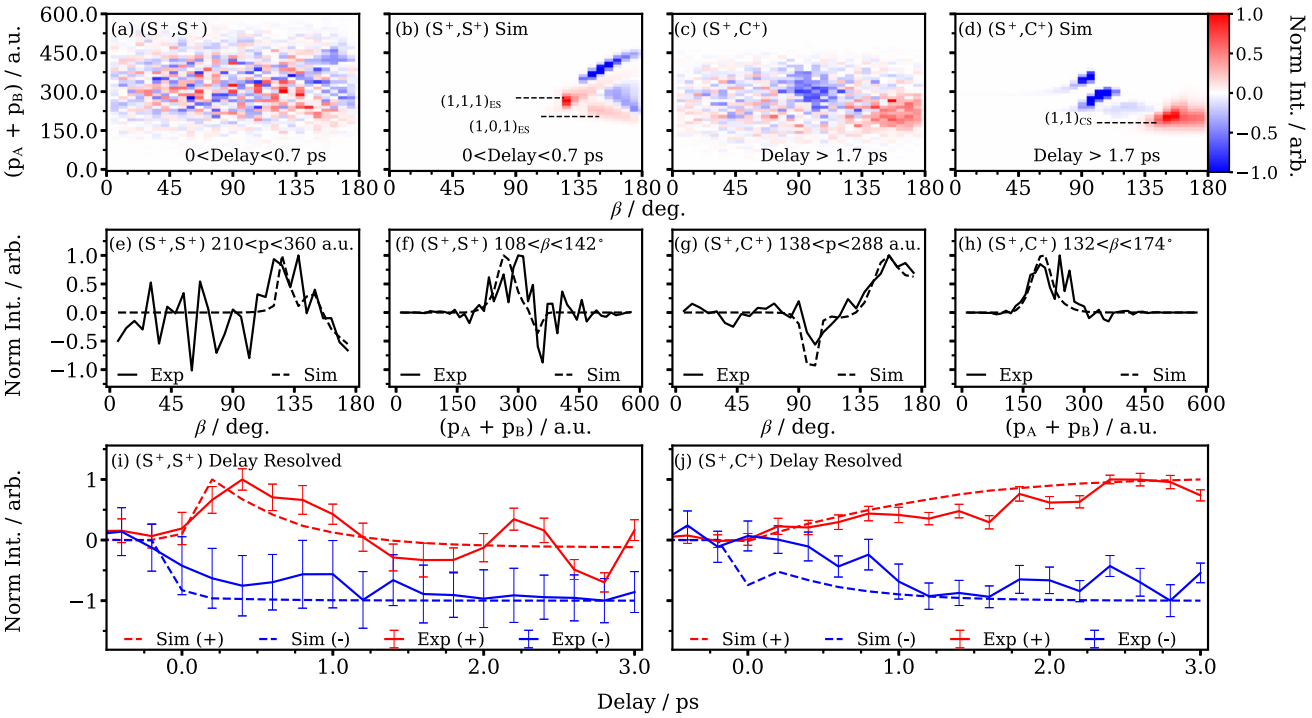

Fig. 3 Delay-dependent three-dimensional covariance analysis. Three-dimensional covariance analysis for ion pairs (S^+,S^+) (**a**, **b**) and (S^+,C^+) (**c**, **d**) performed for the experimental and simulated data.. Data are presented for different delays between the UV pump and soft X-ray probe to highlight relevant features, as indicated. The covariance signals are plotted as a function of β, the relative recoil angle of the two ions, and the sum of their absolute momenta in atomic units. Highlighted in **b** and **d** are excited state and CS photoproduct enhancements (labelled with subscript 'ES' and 'CS', respectively). Panels **e**–**h** show 1-dimensional projections with respect to angle and momentum for both the experimental and simulated data of each ion pair. Panels **i**, **j** show 1-dimensional projections of delay as a function of intensity for both the major enhancements and depletions in each experimental and simulated covariance image. Red corresponds to an enhancement and blue corresponds to a depletion. The angle and momentum regions sampled to produce these projections are shown in Fig. S8 in Supplementary Note 4. The time-dependent covariance intensities were normalised to +/− 1 for the enhancements/depletions, respectively, and the error bars were calculated via bootstrapping analysis, where the standard deviation was determined from 200 re-samplings of the data per delay bin.

simulations. We note that some discrepancy between experiment and simulation is seen in the delay-dependent behaviour of the ground-state depletion at early delay times, shown in Fig. 3j. This arises due to overlap between ground-state signal and transient signal related to the electronically-excited species in the experiment, which is more well separated in the simulation, as shown in Fig. S7.

S^{2+} momentum distributions. Figure 4 shows the experimental (a) and simulated (b) S^{2+} momentum distributions for the S^{2+} ion as a function of pump-probe delay.

As mentioned previously, significant qualitative differences between the S^+ and S^{2+} momentum distributions following photodissociation are expected and observed due to the site-selective S 2p ionisation process, which deposits at least two positive charges per photoabsorption[49]. Thus, signal arising from S 2p ionisation of dissociated S atoms may be observed in the S^{2+} ion. To more clearly show the contributions from different fragmentation channels, Fig. 4c decomposes the simulated delay-dependent S^{2+} momentum distributions by fragmentation channel.

Firstly, akin to the transient feature observed in the S^+ momentum distribution (Fig. 2), a transient enhancement is visible within the first picosecond following excitation and between 190–250 a.u. The lifetime and appearance of this channel is attributed to the same origin as the S^+ transient, that is, a transition to a bent and stretched geometry in the excited state. This can be observed in the simulated fragmentation channels involving Coulomb explosion of bound molecules to a S^{2+} ion, namely Channels 3 and 4 in Fig. 4c. Due to the increased number of fragmentation channels contributing to production of S^{2+}, such signal is more heavily overlapped with other enhancements than in S^+.

Between 80 and 200 a.u., significant variation is observed in the measured momentum across the first few picoseconds, shifting to lower ion momentum at later times. This feature can be linked to a Coulomb explosion of a molecule undergoing photodissociation, as has been noted in several earlier time-resolved CEI studies[6,8,9,18]. At short pump-probe delays (i.e. interatomic distances), we expect additional Coulombic repulsion to contribute significantly to the final ionic momenta when both the S and CS fragments are ionised by the probe pulse. As the delay between dissociation and ionisation is increased, the Coulombic contribution to the observed total momentum decreases and eventually plateaus, giving rise to the 'Coulomb curve' feature. This is clearly observed in Channel 3 (Fig. 4c) for the fragmentation channel in which both S and CS photoproducts are doubly ionised. Additional signal at higher momentum (~100–200 a.u.) persists out to long pump-probe delays, as expected for Coulomb explosion of the CS photoproduct following multiple ionisation into S^{2+}, as demonstrated in the simulations of Channels 2 and 4 (Fig. 4c).

Finally, a low momentum feature is observed between 0 and 80 a.u. with a delayed onset relative to the temporal overlap of the two pulses. This feature can be assigned to double ionisation of dissociated atomic sulfur produced with a neutral CS cofragment, as seen in simulated Channels 1 and 6 (Fig. 4c). Analogous

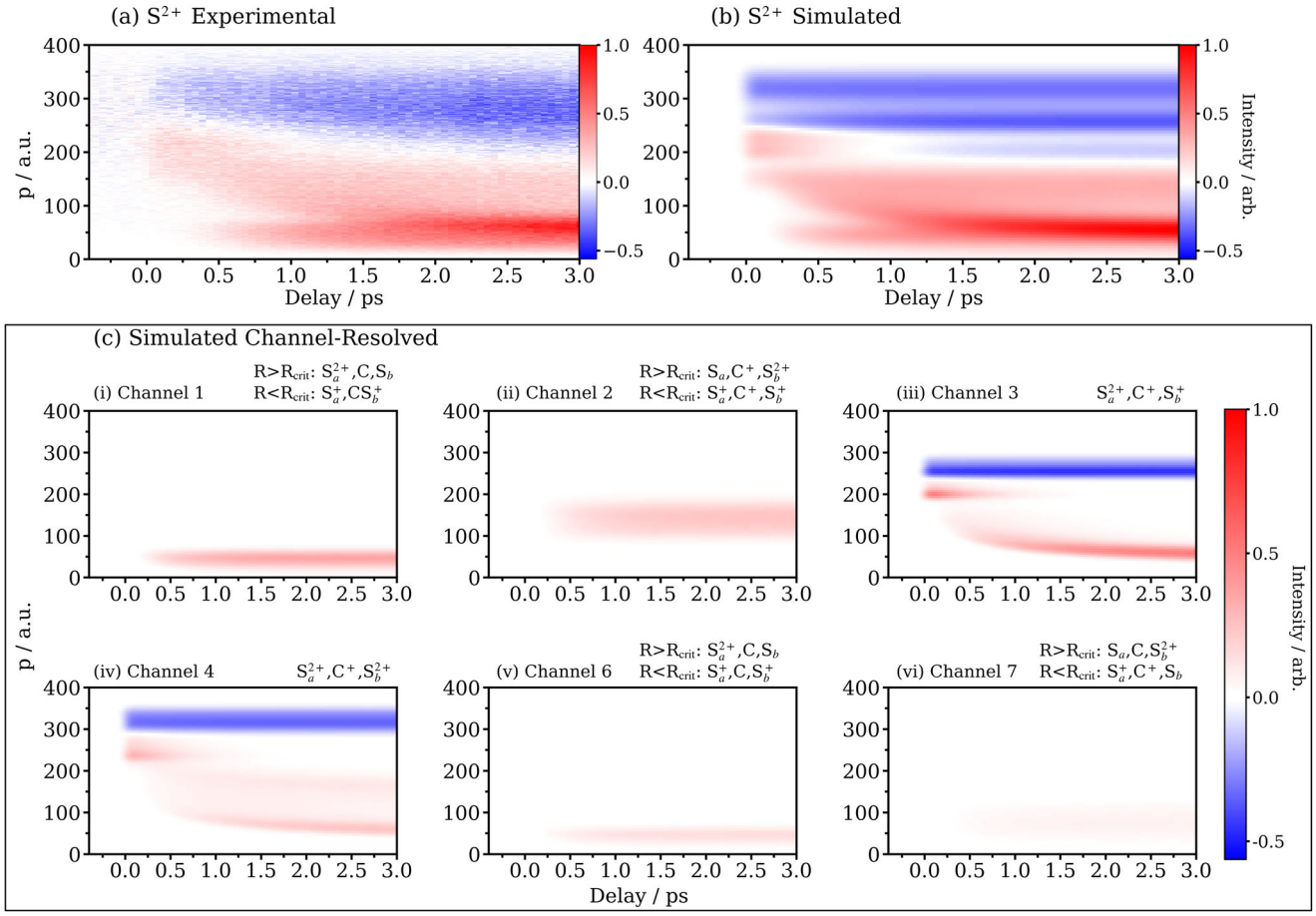

Fig. 4 Experimental and simulated delay-dependent momentum distributions for the S^{2+} ion. Panels **a**, **b** show the full experimental and simulated momentum distributions of S^{2+}. Panel **c** shows the main individual fragmentation channels that contribute to the full S^{2+} simulation. A detailed discussion of methodology used to generate the simulated difference signal as well as assignment of the channels is provided in the S^{2+} Momentum Distributions section. A summary of the relative probabilities of each channel is provided in Table 1. R_{crit} denotes the separation at which the applied fragment charges changes, corresponding to the localisation of charge at either the S or CS site following soft X-ray ionisation. Values of R_{crit} for the different charge transfer processes were calculated using the classical over-the-barrier model and are shown in Table S1 in Supplementary Note 5.

features with the same physical origin were also observed in the S^{3+} and S^{4+} ion momentum distributions, albeit with differing onset times for each charge state. This variation can be linked to charge transfer after localised photoionisation by XUV or X-ray pulses and can occur for greater internuclear separations for higher charge states. Such behaviour has been observed previously in a range of ultrafast photodissociation studies using site-selective XUV or X-ray probing[55–57]. A discussion of the influence of charge transfer dynamics on this channel is provided in Supplementary Note 5.

As noted in the Introduction, the photodissociation of CS_2 involves dynamics occurring via both the singlet and triplet manifolds[31], which lead to somewhat different velocity distributions of the dissociated photoproducts[42,43]. Analysis of the corresponding low momentum (<80 a.u.) feature can provide further insight into the branching between these two channels, owing to different velocity distributions associated with dissociation to either singlet (^{1}D) and triplet (^{3}P) S atom products. A detailed comparison to the nanosecond photodissociation and resonance-enhanced multiphoton ionisation (REMPI) experiments of Brouard and coworkers is provided in Supplementary Note 6[42,43]. In line with several previous studies[31,32], triplet production appears to be favoured, although it should be noted that the expected singlet and triplet velocity distributions heavily overlap, precluding a more detailed channel-resolved analysis.

To conclude, we have presented a time-resolved Coulomb explosion imaging study of UV-excited CS_2, probed by site-selective multiple ionisation with intense soft X-ray pulses. Aided by covariance imaging analysis and modelling, a picture of the complex photoinduced dynamics was extracted from the recorded delay-dependent ion momentum distributions. This involves rapid motion along stretching and bending coordinates prior to dissociation to CS + S on longer timescales, consistent with previous spectroscopic measurements. Observed covariant ion momentum distributions arising from Coulomb explosion of the bound excited state, consistent with our modelling for a distribution of geometries with a mean bond angle of 135°, directly confirm the previously assumed bent and stretched excited-state structure. Our study thus represents a key step in the development of CEI as a tool for structural imaging of photoexcited systems, particularly through exploiting the high sensitivity of CEI to bond angles[11,21,58,59], the evolution of which is crucial in the photochemistry of CS_2. This ability to extract bond angles of photoexcited species remains a challenge for diffractive imaging techniques, which are generally sensitive to the distances between pairs of scatterers[4,5,36,37]. It should be noted that the current experiment was operated at 10 Hz, as limited by the repetition rate of the FLASH pump-probe laser. Ongoing developments in high-repetition rate (kHz-MHz) FELs will allow the full exploitation of multi-dimensional covariance imaging techniques[51,60–62].

This will extract fully channel-resolved correlated momentum distributions for different Coulomb explosion channels, providing rich structural dynamical information, even for larger molecules. Future work can also exploit recent developments in electron-ion covariance analysis[63] to disentangle the nuclear and electronic contributions to emerging inner-shell photoelectron spectroscopic measurements[13,63,64], by extracting spectra associated with a specific Coulomb explosion signature, and thus a group of nuclear structures.

Methods

Experimental. Time-resolved CEI measurements on CS_2 were conducted at the CAMP@FLASH instrument[65] on beamline BL1 at the Free-electron LASer in Hamburg (FLASH)[66]. Isolated CS_2 molecules were delivered into the chamber as a continuous supersonic jet, perpendicularly intersecting the pump and probe pulses. A double-sided velocity map imaging (VMI) spectrometer was used to record the three-dimensional momenta of charged ions following multiple ionisation by the FEL. The current work focuses on the ion data collected, while a separate manuscript follows the photodynamics through time-resolved photoelectron spectroscopy[13]. The VMI spectrometer used a detector comprising two stacked micro-channel plates (MCP) in a chevron configuration and a P47 phosphor screen. Electrodes set to velocity mapping potentials directed ions formed in the interaction region along the time-of-flight tube onto this detector. Resulting hits on the P47 screen were recorded using a Timepix3 camera from Amsterdam Scientific Instruments, which was equipped with a 256×256 pixel sensor. In addition to the positional information, the camera can also record the pixel time-of-arrival and time-over-threshold with a 1.56 ns and 25 ns precision, respectively[67]. The temporal and spatial resolution was improved via centroiding, as described for the CAMP setup by Bromberger et al.[68]. When coupled with the x and y detector position of each ion, this permitted the reconstruction of three-dimensional momenta. Calibration of the fragment momenta was obtained using ion trajectory simulations in SIMION 8.1.

The optical arrangement used in this experiment is similar to ref. [56], which contains a detailed description of the optical setup. Briefly, the UV pump pulse was generated as the fourth harmonic of a 55 fs, 12 mJ, 800 nm near-infrared (NIR) pulse as follows: two β-BaB_2O_4 (BBO) crystals were used to frequency triple 50% of the NIR beam and dichroic mirrors were then used to isolate the resultant third harmonic. Sum-frequency mixing of the third harmonic with 25% of the original NIR beam (obtained using two successive 50:50 beam splitters) then yielded the fourth harmonic. The resultant UV pulse (201.5 ± 0.4 nm, 0.45 μJ) was steered into the interaction region by three successive mirrors with a total reflectivity of 48%, giving a pulse energy of 0.22 μJ at the interaction region. The temporal duration of the 201.5 nm pump pulse was determined via two colour non-resonant multiphoton ionisation of Xe with another NIR pulse within the VMI instrument. A UV/NIR cross-correlation of 150 fs was obtained from this data, which gives a lower limit of the 201.5 nm pulse duration of 140 fs. Taking a previously determined focal spot diameter of 30 μm, and accounting for the reflectivity of the mirrors, we estimate a peak UV intensity at the interaction region of 2.1×10^{11} Wcm^{-2}.

Intense soft X-ray pulses from FLASH were used to site-selectively ionise and Coulomb explode CS_2 by tuning the photon energy to ~180 eV (~6.9 nm), above the S 2p edge[48]. Photoionisation of this core orbital predominantly double ionises CS_2, with a non-negligible contribution from triple ionisation[49]. The FEL operated with an average pulse energy of 54 ± 10 μJ. Accounting for the losses from transmission along the beamline, this gives an average FEL pulse energy in the interaction region of 23 μJ. Fluctuations in the FEL pulse energy and timing were tracked on a shot-to-shot basis using the measurements of the Gas Monitor Detector (GMD)[69] and the Bunch Arrival Monitor (BAM)[70], respectively. Based on measurements of the electron bunch charge, photon spectra and the transverse deflecting cavity 'LOLA', the soft X-ray pulse duration was inferred to be approximately 90 fs[71]. Assuming a focal spot size of 10 μm, this gives a soft X-ray intensity of 7.2×10^{14} Wcm^{-2}. The optical laser was overlapped with the soft X-ray probe pulse via a drilled aluminium mirror and recombined in a near collinear geometry. The delay between the UV and soft X-ray pulses was adjusted using a computer controlled delay stage placed in the NIR beampath before the UV generation scheme. Data were recorded at 10 Hz, the repetition rate of the optical and free-electron lasers. The temporal overlap, t_0, between the UV and soft X-ray pulses was determined by examining the onset time for production of high momentum C^+ and C^{2+}, which yielded a rapid enhancement after UV photoexcitation of CS_2. Monitoring various ion transient features on a scan-by-scan basis allowed for any temporal drifts not captured by the BAM to be accounted for.

Three-dimensional contingent covariance. By recording the three-dimensional momenta of many ions per FEL shot, correlations between the relative fragment momenta can be determined. In many experiments these correlations are determined through coincidence analysis, which relies on operating at sufficiently low count rates to ensure that on average only a single target molecule is ionised per shot. Under our experimental conditions, an average of ~84 ions were recorded per shot, making such analysis impossible. However, correlated information can still be extracted through covariance analysis[50]. For two ions, A and B, the covariance, a measurement of linear correlation, is calculated as shown in Eq. (1):

$$\mathrm{Cov}(X_A, X_B) = \langle X_A - \langle X_A \rangle \rangle \langle X_B - \langle X_B \rangle \rangle \quad (1)$$

where $\langle X \rangle$ refers to the mean of the measured quantity X (ion counts) over a series of observations (laser shots). We exploit a three-dimensional covariance imaging method, outlined in detail in ref. [51], to extract correlations between ions as a function of their relative three-dimensional momenta. An extension to this methodology, when conducting experiments at self-amplified spontaneous emission (SASE) FELs, is to account for large inherent shot-by-shot fluctuations in the soft X-ray pulse properties[72–75]. We apply a contingent covariance approach (see ref. [53,76]) to suppress false contributions to the calculated covariance from correlations produced due to fluctuating FEL pulse energies, which result in all ions appearing correlated. The data is filtered to exclude the low and high power edges of the FEL pulse energy distribution, and then split into specified pulse energy ranges, each containing an equal number of shots. The covariance calculated for each individual energy range is then combined to produce an overall covariance image. This process is expanded upon in Supplementary Note 10.

The high-dimensional data produced from three-dimensional covariance or coincidence ion imaging experiments can be shown in numerous representations (see, for example, ref. [77]). For the work presented here, we adopt a representation outlined in ref. [51] where the summed magnitude of a pair of fragment momenta is plotted as a function of relative recoil angle (β). The signal is binned uniformally in this angle, with no Jacobian correction applied. For a triatomic molecular system such as CS_2, this has been shown to be an efficient way to track bending during evolving structural dynamics[51,77].

Coulomb explosion imaging simulations. The individual channels belonging to the momentum distributions of each ion were identified by comparison to Coulombic simulations. These were generated in the following manner. Firstly, for 10^4 molecules the photoexcitation process was simulated by assuming prompt population of an excited state, which decayed to a dissociating state with an exponential time constant of 500 fs.

The simulations use representative static distributions of geometries (as explained below) for the ground, excited and dissociated CS_2 states. The CEI results are modelled by manually fitting a set of fragmentation channels and the minimum number of fragmentation channels were utilised to account for all major features. Increasing the quantity of channels would further improve the simulation, but would also greatly increase the difficulty of fitting the probability of each individual channel. For each simulated trajectory, the system is propagated between −500 and 0 fs to provide a background signal and between 0 and 3000 fs to provide a time-dependent signal, and at each time delay Coulomb exploded to model the experimental observables. If a trajectory is yet to be photoexcited, Coulomb explosion occurs from a distribution of geometries representing unpumped molecules. A distribution of bent and stretched geometries is instead used for molecules that are photoexcited but not yet dissociated. The bend angle used for this distribution was determined from the experimental covariance data. The relevant geometry distributions are given in Table 2. After dissociation, the S and CS fragments are set to recoil from one another with a constant dissociation velocity. The dissociation velocity was sampled from a Gaussian kinetic energy distribution based upon the experimentally observed distribution of dissociated sulfur atoms. Additionally, available kinetic energy not partitioned into translational energy is assumed to be partitioned into rotation of the CS fragment, which is also accounted for in the dissociation simulation, leading to a rapidly evolving S-C-S bond angle following dissociation. Relevant structural parameters used in the simulations are given in Table 2. A mean bend angle of the ground state that is smaller than 180° was used, as is expected for a thermal distribution of a triatomic molecule with a linear equilibrium structure and discussed in detail by Jensen et al. for the specific case of CO_2[78]. The earlier work of Hasegawa et al. computed an expected mean bend angle of 174° for the vibrational ground level of the electronic ground state of CS_2[79]. In their NIR-induced CEI study, however, a mean angle of 145° was observed. The better agreement of the mean angle extracted in the present work to the expected value may be due to the use of the soft X-ray probe, which eliminates bending motion prior to Coulomb explosion caused by field-induced couplings of different electronic states[79].

At each time delay in the simulation, Coulomb explosion was modelled by treating ions as Coulombically repelling classical point charges. For the case of a two-body Coulomb explosion of bound CS_2 into $CS^+ + S^+$, the point charge in the CS^+ fragment was located on the S^+ atom. For experimentally observed Coulomb explosion channels involving a neutral fragment (e.g., the (1,0,1) and (1,1,0) channels), which cannot be adequately described considering single point charges, a small partial positive charge (uniformly sampled between +0.05 and +0.3) was assigned to the neutral fragment. This assumption yielded qualitative agreement with the experimentally observed data for these channels. This produced sets of differential equations that were numerically integrated, with time steps of 1 fs for the first 400 fs, and subsequent steps of 50 fs out to 5 ps. This outputs a final momentum for each fragment following the Coulomb explosion. For the plotting of simulated delay-dependent momentum distributions, the data were convoluted in pump-probe delay by a Gaussian function of $\sigma = 50$ fs to emulate the experimental time resolution. Several Coulomb explosion channels were included with ions in initially stationary geometries, and were randomly sampled with different weightings, as listed in Table 1. These weightings were determined by empirically by adjusting the weight of each channel to obtain satisfactory agreement with the experimental data. To account for differences in the localisation of charge following S 2p ionisation in bound CS_2 molecules or dissociated S and CS fragments, differing charge state distributions were used in the limit of short and long S-CS bond lengths. In the simulation, this 'critical distance', beyond which charge remains localised at the ionised fragment, was set at a bond length of 5.5 Å. A single value of this critical distance was chosen due to simplicity in the modelling. Supplementary Note 5 gives critical distances predicted by a classical over-the-barrier model[55,80] for a series of possible ionisation and charge transfer pathways. The modelling neglects any contributions from single valence ionisation by the probe pulse, as well as the possibility of producing stable CS^{2+} following S 2p ionisation and Auger-Meitner decay. As such, molecular charged CS^{n+} fragments are not produced following dissociation and S 2p ionisation in the model. The effects of varying each of the above mentioned simulation parameters are shown in Supplementary Note 8.

Table 2 Structural parameters used in the Coulomb explosion simulations.

Parameter	Mean ± Standard Deviation
Equilibrium C-S length	1.55Å ± 0.1Å[79]
Equilibrium S-C-S angle	165.5° ± 9°
Excited, bent C-S length	2.2Å ± 0.5Å
Excited, bent S-C-S angle	135° ± 40°
Dissociated C-S length	1.8Å ± 0.4Å

Mean and standard deviation of the structural parameters used for the CS_2 Coulomb explosion simulations for ground, excited and bent, and dissociated states.

Data availability

The data that support the findings of this study are available from the corresponding author on request. All steps to reproduce the presented experimental and theoretical findings are either explained in detail or cited in the manuscript.

Code availability

The codes used to process and analyse the experimental data are available from the corresponding authors on request. The codes to generate the simulated Coulomb explosion are available via an online repository[81].

Received: 12 April 2023; Accepted: 4 October 2023;
Published online: 20 October 2023

References

1. Kukura, P., McCamant, D. W., Yoon, S., Wandschneider, D. B. & Mathies, R. A. Structural observation of the primary isomerization in vision with femtosecond-stimulated Raman. *Science* **310**, 1006–1009 (2005).
2. Zaharieva, I., Dau, H. & Haumann, M. Sequential and coupled proton and electron transfer events in the $S_2 \rightarrow S_3$ transition of photosynthetic water oxidation revealed by time-resolved X-ray absorption spectroscopy. *Biochem* **55**, 6996–7004 (2016).
3. Stolow, A., Bragg, A. E. & Neumark, D. M. Femtosecond time-resolved photoelectron spectroscopy. *Chem. Rev.* **104**, 1719–1758 (2004).
4. Xu, J., Blaga, C. I., Agostini, P. & DiMauro, L. F. Time-resolved molecular imaging. *J. Phys. B: ., Mol. Opt. Phys.* **49**, 112001 (2016).
5. Odate, A., Kirrander, A., Weber, P. M. & Minitti, M. P. Brighter, faster, stronger: ultrafast scattering of free molecules. *Adv. Phys.: X* **8**, 2126796 (2023).

6. Stapelfeldt, H., Constant, E. & Corkum, P. B. Wave packet structure and dynamics measured by Coulomb explosion. *Phys. Rev. Lett.* **74**, 3780–3783 (1995).
7. Légaré, F., Lee, K. F., Bandrauk, A. D., Villeneuve, D. M. & Corkum, P. B. Laser Coulomb explosion imaging for probing ultra-fast molecular dynamics. *J. Phys. B: ., Mol. Opt. Phys.* **39**, S503 (2006).
8. Allum, F. et al. Coulomb explosion imaging of CH_3I and CH_2ClI photodissociation dynamics. *J. Chem. Phys.* **149**, 204313 (2018).
9. Burt, M. et al. Coulomb-explosion imaging of concurrent CH_2BrI photodissociation dynamics. *Phys. Rev. A* **96**, 043415 (2017).
10. Endo, T. et al. Capturing roaming molecular fragments in real time. *Science* **370**, 1072–1077 (2020).
11. Boll, R. et al. X-ray multiphoton-induced Coulomb explosion images complex single molecules. *Nat. Phys.* **18**, 423–428 (2022).
12. Neville, S. P. et al. Beyond structure: ultrafast X-ray absorption spectroscopy as a probe of non-adiabatic wavepacket dynamics. *Faraday Discuss.* **194**, 117–145 (2016).
13. Gabalski, I. et al. Time-resolved x-ray photoelectron spectroscopy: ultrafast dynamics in cs_2 probed at the s 2p edge. *J. Phys. Chem. Lett.* **14**, 7126–7133 (2023).
14. Corrales, M. E. et al. Velocity map imaging and theoretical study of the Coulomb explosion of CH_3I under intense femtosecond ir pulses. *J. Phys. Chem. A* **116**, 2669–2677 (2012).
15. Luzon, I., Livshits, E., Gope, K., Baer, R. & Strasser, D. Making sense of Coulomb explosion imaging. *J. Phys. Chem. Lett.* **10**, 1361–1367 (2019).
16. Zhou, W. et al. Coulomb explosion imaging for gas-phase molecular structure determination: An ab initio trajectory simulation study. *J. Chem. Phys.* **153**, 184201 (2020).
17. Malakar, Y. et al. Time-resolved imaging of bound and dissociating nuclear wave packets in strong-field ionized iodomethane. *Phys. Chem. Chem. Phys.* **21**, 14090–14102 (2019).
18. Ding, X. et al. Threshold photodissociation dynamics of NO_2 studied by time-resolved cold target recoil ion momentum spectroscopy. *J. Chem. Phys.* **151**, 174301 (2019).
19. Ibrahim, H. et al. Tabletop imaging of structural evolutions in chemical reactions demonstrated for the acetylene cation. *Nat. Commun.* **5**, 4422 (2014).
20. Bocharova, I. et al. Charge resonance enhanced ionization of CO_2 probed by laser Coulomb explosion imaging. *Phys. Rev. Lett.* **107**, 063201 (2011).
21. Légaré, F. et al. Laser Coulomb-explosion imaging of small molecules. *Phys. Rev. A* **71**, 013415 (2005).
22. Bucksbaum, P. H., Zavriyev, A., Muller, H. G. & Schumacher, D. W. Softening of the H_2^+ molecular bond in intense laser fields. *Phys. Rev. Lett.* **64**, 1883 (1990).
23. Seideman, T., Ivanov, M. Y. & Corkum, P. B. Role of electron localization in intense-field molecular ionization. *Phys. Rev. Lett.* **75**, 2819 (1995).
24. Li, X. et al. Coulomb explosion imaging of small polyatomic molecules with ultrashort X-ray pulses. *Phys. Rev. Res.* **4**, 013029 (2022).
25. Hishikawa, A., Hasegawa, H. & Yamanouchi, K. Sequential three-body Coulomb explosion of CS_2 in intense laser fields appearing in momentum correlation map. *Chem. Phys. Lett.* **361**, 245–250 (2002).
26. Hishikawa, A., Hasegawa, H. & Yamanouchi, K. Nuclear dynamics on the light-dressed potential energy surface of CS_2 by coincidence momentum imaging. *Chem. Phys. Lett.* **388**, 1–6 (2004).
27. Wang, X., Zhang, J., Zhang, S.-A. & Sun, Z.-R. Coulomb explosion of CS_2 molecule under an intense femtosecond laser field. *Chin. Phys. B* **25**, 053301 (2016).
28. Hishikawa, A., Iwamae, A. & Yamanouchi, K. Ultrafast deformation of the geometrical structure of CO_2 induced in intense laser fields. *Phys. Rev. Lett.* **83**, 1127 (1999).
29. Kono, H., Koseki, S., Shiota, M. & Fujimura, Y. A theoretical study of electronic dynamics and deformation of CO_2 in intense laser fields. *J. Phys. Chem. A* **105**, 5627–5636 (2001).
30. Endo, T. et al. Selective bond breaking of CO_2 in phase-locked two-color intense laser fields: laser field intensity dependence. *Phys. Chem. Chem. Phys.* **19**, 3550–3556 (2017).
31. Mank, A., Starrs, C., Jego, M. & Hepburn, J. A detailed study of the predissociation dynamics of the $^1B_2$ ($^1\Sigma_u^+$) state of CS_2. *J. Chem. Phys.* **104**, 3609–3619 (1996).
32. Karashima, S., Suzuki, Y.-I. & Suzuki, T. Ultrafast extreme ultraviolet photoelectron spectroscopy of nonadiabatic photodissociation of CS_2 from $^1B_2$ ($^1\Sigma_u^+$) state: Product formation via an intermediate electronic state. *J. Phys. Chem. Lett.* **12**, 3755–3761 (2021).
33. Smith, A. D. et al. Mapping the complete reaction path of a complex photochemical reaction. *Phys. Rev. Lett.* **120**, 183003 (2018).
34. Hockett, P., Bisgaard, C., Clarkin, O. & Stolow, A. Time-resolved imaging of purely valence-electron dynamics during a chemical reaction. *Nat. Phys.* **7**, 612–615 (2011).
35. Bisgaard, C. Z. et al. Time-resolved molecular frame dynamics of fixed-in-space CS_2 molecules. *Science* **323**, 1464–1468 (2009).
36. Razmus, W. O. et al. Multichannel photodissociation dynamics in CS_2 studied by ultrafast electron diffraction. *Phys. Chem. Chem. Phys.* **24**, 15416–15427 (2022).
37. Gabalski, I. et al. Transient vibration and product formation of photoexcited CS_2 measured by time-resolved x-ray scattering. *J. Chem. Phys.* **157**, 164305 (2022).
38. Kitsopoulos, T. N., Gebhardt, C. R. & Rakitzis, T. P. Photodissociation study of CS_2 at 193 nm using slice imaging. *J. Chem. Phys.* **115**, 9727–9732 (2001).
39. Farmanara, P., Stert, V. & Radloff, W. Ultrafast predissociation and coherent phenomena in CS_2 excited by femtosecond laser pulses at 194-207 nm. *J. Chem. Phys.* **111**, 5338–5343 (1999).
40. Townsend, D. et al. $^1B_2$ ($^1\Sigma_u^+$) excited state decay dynamics in CS_2. *J. Chem. Phys.* **125**, 234302 (2006).
41. Fuji, T., Suzuki, Y.-I., Horio, T. & Suzuki, T. Excited-state dynamics of CS_2 studied by photoelectron imaging with a time resolution of 22 fs. *Chem. Asian J.* **6**, 3028–3034 (2011).
42. Campbell, E. *Atomic polarisation in molecular photodissociation*. Ph.D. thesis. (University of Oxford, 2011).
43. Brouard, M., Campbell, E. K., Cireasa, R., Johnsen, A. J. & Yuen, W.-H. The ultraviolet photodissociation of CS_2: The S($^1D_2$) channel. *J. Chem. Phys.* **136**, 044310 (2012).
44. Zhao, M. et al. Photodissociation dynamics of CS_2 near 204 nm: The S(^3P_j) +CS($X^1\Sigma^+$) channels. *Chin. J. Chem. Phys.* **34**, 95–101 (2021).
45. Wang, K., McKoy, V., Hockett, P. & Schuurman, M. Time-resolved photoelectron spectra of CS_2: Dynamics at conical intersections. *Phys. Rev. Lett.* **112**, 113007 (2014).
46. Bellshaw, D. et al. Ab-initio surface hopping and multiphoton ionisation study of the photodissociation dynamics of CS_2. *Chem. Phys. Lett.* **683**, 383–388 (2017).
47. Bellshaw, D., Minns, R. S. & Kirrander, A. Correspondence between electronic structure calculations and simulations: Nonadiabatic dynamics in cs 2. *Phys. Chem. Chem. Phys.* **21**, 14226–14237 (2019).
48. Siggel, M. R. F., Field, C., Sæthre, L. J., Bøørve, K. J. & Thomas, T. D. High resolution photoelectron spectroscopy of sulfur 2p electrons in H_2S, SO_2, CS_2, and OCS. *J. Chem. Phys.* **105**, 9035–9039 (1996).
49. Eland, J. et al. Spectra of the triply charged ion CS_2^{3+} and selectivity in molecular Auger effects. *J. Chem. Phys.* **132**, 104311 (2010).
50. Frasinski, L. J., Codling, K. & Hatherly, P. A. Covariance mapping: A correlation method applied to multiphoton multiple ionization. *Science* **246**, 1029–1031 (1989).
51. Allum, F. et al. Multi-particle three-dimensional covariance imaging: “coincidence" insights into the many-body fragmentation of strong-field ionized D_2O. *J. Phys. Chem. Lett.* **12**, 8302–8308 (2021).
52. Guillemin, R. et al. Selecting core-hole localization or delocalization in CS_2 by photofragmentation dynamics. *Nat. Commun.* **6**, 6166 (2015).
53. McManus, J. W. et al. Disentangling sequential and concerted fragmentations of molecular polycations with covariant native frame analysis. *Phys. Chem. Chem. Phys.* **24**, 22699–22709 (2022).
54. Wang, K., McKoy, V., Hockett, P., Stolow, A. & Schuurman, M. S. Monitoring non-adiabatic dynamics in CS_2 with time- and energy-resolved photoelectron spectra of wavepackets. *Chem. Phys. Lett.* **683**, 579–585 (2017).
55. Erk, B. et al. Imaging charge transfer in iodomethane upon x-ray photoabsorption. *Science* **345**, 288–291 (2014).
56. Forbes, R. et al. Time-resolved site-selective imaging of predissociation and charge transfer dynamics: the CH_3I B-band. *J. Phys. B: ., Mol. Opt. Phys.* **53**, 224001 (2020).
57. Allum, F. et al. Multi-channel photodissociation and XUV-induced charge transfer dynamics in strong-field-ionized methyl iodide studied with time-resolved recoil-frame covariance imaging. *Faraday Discuss.* **228**, 571–596 (2021).
58. Christensen, L. et al. Dynamic stark control of torsional motion by a pair of laser pulses. *Phys. Rev. Lett.* **113**, 073005 (2014).
59. Pathak, S. et al. Differentiating and quantifying gas-phase conformational isomers using Coulomb explosion imaging. *J. Phys. Chem. Lett.* **11**, 10205–10211 (2020).
60. Pickering, J. D. et al. Communication: Three-fold covariance imaging of laser-induced Coulomb explosions. *J. Chem. Phys.* **144**, 161105 (2016).
61. Frasinski, L. J. Cumulant mapping as the basis of multi-dimensional spectrometry. *Phys. Chem. Chem. Phys.* **24**, 20776–20787 (2022).
62. Cheng, C. et al. Multiparticle cumulant mapping for Coulomb explosion imaging. *Phys. Rev. Lett.* **130**, 093001 (2023).
63. Allum, F. et al. A localized view on molecular dissociation via electron-ion partial covariance. *Commun. Chem.* **5**, 42 (2022).
64. Braußе, F. et al. Time-resolved inner-shell photoelectron spectroscopy: From a bound molecule to an isolated atom. *Phys. Rev. A* **97**, 043429 (2018).

65. Erk, B. et al. CAMP@FLASH: an end-station for imaging, electron-and ion-spectroscopy, and pump-probe experiments at the FLASH free-electron laser. *J. Synchrotron Radiat.* **25**, 1529–1540 (2018).
66. Ackermann, W. A. et al. Operation of a free-electron laser from the extreme ultraviolet to the water window. *Nat. Photon.* **1**, 336–342 (2007).
67. Nomerotski, A. Imaging and time stamping of photons with nanosecond resolution in timepix based optical cameras. *Nucl. Instrum. Methods Phys. Res. A: Accel. Spectrom. Detect. Assoc. Equip.* **937**, 26–30 (2019).
68. Bromberger, H. et al. Shot-by-shot 250 kHz 3D ion and MHz photoelectron imaging using Timepix3. *J. Phys. B: ., Mol. Opt. Phys.* **55**, 144001 (2022).
69. Tiedtke, K. et al. Gas detectors for X-ray lasers. *J. Appl. Phys.* **103**, 094511 (2008).
70. Schulz, S. et al. Femtosecond all-optical synchronization of an X-ray free-electron laser. *Nat. Commun.* **6**, 5938 (2015).
71. Behrens, C. et al. Constraints on photon pulse duration from longitudinal electron beam diagnostics at a soft x-ray free-electron laser. *Phys. Rev. Accel. Beams.* **15**, 030707 (2012).
72. Mikosch, J. & Patchkovskii, S. Coincidence and covariance data acquisition in photoelectron and-ion spectroscopy. I. formal theory. *J. Mod. Opt.* **60**, 1426–1438 (2013).
73. Mikosch, J. & Patchkovskii, S. Coincidence and covariance data acquisition in photoelectron and-ion spectroscopy. II. analysis and applications. *J. Mod. Opt.* **60**, 1439–1451 (2013).
74. Kornilov, O. et al. Coulomb explosion of diatomic molecules in intense XUV fields mapped by partial covariance. *J. Phys. B: ., Mol. Opt. Phys.* **46**, 164028 (2013).
75. Frasinski, L. J. Covariance mapping techniques. *J. Phys. B: ., Mol. Opt. Phys.* **49**, 152004 (2016).
76. Zhaunerchyk, V., Frasinski, L. J., Eland, J. H. D. & Feifel, R. Theory and simulations of covariance mapping in multiple dimensions for data analysis in high-event-rate experiments. *Phys. Rev. A* **89**, 053418 (2014).
77. Cheng, C. et al. Strong-field ionization of water. II. electronic and nuclear dynamics en route to double ionization. *Phys. Rev. A* **104**, 023108 (2021).
78. Jensen, P., Spanner, M. & Bunker, P. The CO_2 molecule is never linear. *J. Mol. Struct.* **1212**, 128087 (2020).
79. Hasegawa, H., Hishikawa, A. & Yamanouchi, K. Coincidence imaging of Coulomb explosion of CS_2 in intense laser fields. *Chem. Phys. Lett.* **349**, 57–63 (2001).
80. Niehaus, A. A classical model for multiple-electron capture in slow collisions of highly charged ions with atoms. *J. Phys. B: ., Mol. Opt. Phys.* **19**, 2925 (1986).
81. Allum, F., Unwin, J., Burt, M. & Forbes, R. Classical Simulation Code for "X-ray Induced Coulomb Explosion Imaging of Transient Excited- State Structural Rearrangements in CS2" https://doi.org/10.5281/zenodo.8378622 (2023).

Acknowledgements

We acknowledge DESY (Hamburg, Germany), a member of the Helmholtz Association HGF, for the provision of experimental facilities. Parts of this research were carried out at FLASH beamline BL1. Beamtime was allocated for proposal F-20200773. The research leading to this result has been supported by the project CALIPSOplus under the Grant Agreement 730872 from the EU Framework Programme for Research and Innovation HORIZON 2020. The authors gratefully acknowledge the work of the scientific and technical teams at FLASH. We acknowledge the Max Planck Society for funding the development and the initial operation of the CAMP end-station within the Max Planck Advanced Study Group at CFEL and for providing this equipment for CAMP@FLASH. The installation of CAMP@FLASH was partially funded by the BMBF Grants 05K10KT2, 05K13KT2, 05K16KT3 and 05K10KTB from FSP-302. R.F. and F.A. gratefully acknowledge support from the Linac Coherent Light Source, SLAC National Accelerator Laboratory, which is supported by the US Department of Energy, Office of Science, Office of Basic Energy Sciences, under contract no. DE-AC02-76SF00515. P.B. was supported by the U.S. Department of Energy, Office of Science, Basic Energy Sciences (BES), Chemical Sciences, Geosciences, and Biosciences Division, AMOS Program. D.R. was supported by contract no. DE-FG02-86ER13491 from the same funding agency. J.U., T.W., and M.Bu. are grateful for support from the UK EPSRC (EP/S028617/1). J.U. and T.W. are also grateful to the States of Jersey and the EPSRC, respectively, for studentship funding. J.W.L.L. acknowledges financial support from the Helmholtz-ERC Recognition Award (ERC-RA-0043) of the Helmholtz Association (HGF). W.O.R. thanks the STFC XFEL Physical Sciences Hub and the university of Southampton for a PhD studentship. R.S.M. gratefully acknowledges financial support from the Leverhulme Trust via grant RPG-2021-257. M.Br. and C.V. gratefully acknowledge the support of EPSRC Programme Grant EP/V026690/1. I.G. was supported by an NDSEG Fellowship. D.M.P.H. is grateful to the Science and Technology Facilities Council (United Kingdom) for financial support. J.Mik. gratefully acknowledges funding from the European Research Council (ERC) under the European Union's Horizon 2020 research and innovation programme within a Consolidator Grant (CoG agreement No. 101003142). A.S. and P.H. thank the NRC-CSTIP Quantum Sensors grant #QSP-075-1 for financial support. A.S. thanks the NRC-uOttawa Joint Centre for Extreme Photonics (JCEP) and the NSERC (Canada) Discovery Grant Program for financial support. A CC-BY license is applied to the author accepted manuscript arising from this submission, in accordance with UKRI open access conditions.

Author contributions

The experiment was conceived by R.F., benefited from further input from F.A., B.E. and D.R.. The experiments took place during a remote beamtime at the FLASH facility. The experiment was conducted by H.B., N.E., D.G., E.G., S.K., C.Pap., C.Pas., A.S., A.T.N., J. Mik., A.Röd., A.Rou. and B.E. J.U., F.A., M.Bri., I.G., T.D., D.H., A.J.H., P.H., C-S.L., J.W.L.L., J.M., D.M., W.O.R., T.W. provided online data analysis during the experiment. The experimental data was post-analysed by F.A., M.Bri. and J.U., and the simulations developed by F.A. The interpretation of the data was informed by discussions involving J.U., F.A., I.G., M.Bro., P.H.B., D.M.P.H., R.S.M., M.Schu., A.Sto., C.V., D.R., B.E., M.Bu., R.F. Theoretical support was provided by M.Schu. Manuscript preparation was conducted by F.A., M.Bu., R.F., D.R. and J.U. with input from all authors.

Competing interests

The authors declare no competing interests.

Additional information

Supplementary information The online version contains supplementary material available at https://doi.org/10.1038/s42005-023-01414-7.

Correspondence and requests for materials should be addressed to Felix Allum, Michael Burt or Ruaridh Forbes.

Peer review information *Communications Physics* thanks the anonymous reviewers for their contribution to the peer review of this work. A peer review file is available.

Reprints and permission information is available at http://www.nature.com/reprints

Publisher's note Springer Nature remains neutral with regard to jurisdictional claims in published maps and institutional affiliations.